AGU PUBLICATIONS

JGR

Journal of Geophysical Research: Atmospheres

RESEARCH ARTICLE
10.1002/2017JD027080

Key Points:
- Characteristics of the convectively driven cold layer observed from GPS RO data
- Dehydration of the TTL by the convectively driven cold layer
- Transient circulation response to deep convection helps dehydration process in the TTL

Supporting Information:
- Supporting Information S1

Correspondence to:
J. Kim,
joowan.k@gmail.com

Citation:
Kim, J., Randel, W. J., & Birner, T. (2018). Convectively driven tropopause-level cooling and its influences on stratospheric moisture. *Journal of Geophysical Research: Atmospheres, 123*. https://doi.org/10.1002/2017JD027080

Received 4 MAY 2017
Accepted 22 DEC 2017
Accepted article online 28 DEC 2017

©2017. American Geophysical Union. All Rights Reserved.

Convectively Driven Tropopause-Level Cooling and Its Influences on Stratospheric Moisture

Joowan Kim[1,2,3], William J. Randel[1], and Thomas Birner[2]

[1]National Center for Atmospheric Research, Boulder, CO, USA, [2]Department of Atmospheric Science, Colorado State University, Fort Collins, CO, USA, [3]Now at Department of Atmospheric Science, Kongju National University, Gongju, South Korea

Abstract Characteristics of the tropopause-level cooling associated with tropical deep convection are examined using CloudSat radar and Constellation Observing System for Meteorology, Ionosphere and Climate (COSMIC) GPS radio occultation measurements. Extreme deep convection is sampled based on the cloud top height (>17 km) from CloudSat, and colocated temperature profiles from COSMIC are composited around the deep convection. Response of moisture to the tropopause-level cooling is also examined in the upper troposphere and lower stratosphere using microwave limb sounder measurements. The composite temperature shows an anomalous warming in the troposphere and a significant cooling near the tropopause (at 16–19 km) when deep convection occurs over the western Pacific, particularly during periods with active Madden-Julian Oscillation (MJO). The composite of the tropopause cooling has a large horizontal scale (~6,000 km in longitude) with minimum temperature anomaly of ~ −2 K, and it lasts more than 2 weeks with support of mesoscale convective clusters embedded within the envelope of the MJO. The water vapor anomalies show strong correlation with the temperature anomalies (i.e., dry anomaly in the cold anomaly), showing that the convectively driven tropopause cooling actively dehydrate the lower stratosphere in the western Pacific region. The moisture is also affected by anomalous Matsuno-Gill-type circulation associated with the cold anomaly, in which dry air spreads over a wide range in the tropical tropopause layer (TTL). These results suggest that convectively driven tropopause cooling and associated transient circulation play an important role in the large-scale dehydration process in the TTL.

Plain Language Summary Convection in the tropics may be expected to hydrate the upper atmosphere. However, over the western Pacific, it dehydrates upper atmosphere by making a significant cooling near the tropopause.

1. Introduction

The amount of water vapor in the stratosphere (SWV) is roughly 4 orders of magnitude smaller than that in the lower troposphere. However, due to its strong radiative impact on the Earth's radiation budget (Forster & Shine 1999, 2002; Solomon et al., 2010), the global distribution, and source and sink mechanisms of SWV are important topics of climate research. The amount of SWV is affected in general by two major processes. One is methane oxidation in the stratosphere (Le Texier et al., 1988), and the other is transport from the troposphere, where SWV is primarily controlled by dehydration processes in the tropical tropopause layer (Fueglistaler et al., 2009; Holton et al., 1995). Methane oxidation contributes to a slow increase in SWV during recent decades due to increased loadings of methane in the stratosphere, and its impact is generally well understood (e.g., Dlugokencky et al., 1998; Fueglistaler & Haynes, 2005).

On the other hand, the details of water vapor transport across the tropical tropopause are less understood and topics of active scientific research (e.g., Jensen et al., 2016; Schoeberl et al., 2016). The primary transport processes occur through the tropical tropopause layer (TTL), where slow large-scale upwelling brings tropospheric air into the lower stratosphere (Holton et al., 1995). Thermal structures and transport pathways in the TTL are important aspects that influence water vapor (e.g., Fueglistaler & Haynes, 2005; Jensen & Pfister, 2004; Mote et al., 1996; Randel et al., 2004). However, because these properties are affected by complex physical and dynamical processes in the TTL (see Fueglistaler et al., 2009; Randel & Jensen, 2013, for detailed overview), observation and evaluation of the transport (and mixing) processes are not simple tasks.

In addition to the large-scale transport processes, extreme deep convection may provide an additional mechanism of transport for SWV. Although only a small portion of deep convection penetrates

background tropopause levels, this overshooting deep convection could directly transport high water content to the lower stratosphere (and hydrate the lower stratosphere). This direct transport mechanism has been observed for isolated cases of extreme convection, based on in situ measurements obtained from aircraft and radiosonde observations (e.g., Corti et al., 2008; Khaykin et al., 2009) and extreme events from satellites (Schwartz et al., 2013).

However, deep convection may play an opposite role on SWV by modulating the thermal structure of the TTL (e.g., Randel et al., 2015). In the tropics, a localized temperature minimum is frequently observed over active convection (e.g., Gettelman et al., 2002; Holloway & Neelin, 2007; Johnson & Kriete, 1982). Particularly, the cold anomaly is generally observed near the cold-point tropopause (CPT) as a thin layer lasting a couple of weeks in boreal winter (Kim & Son, 2012; Paulik & Birner, 2012). This tropopause-level cooling may dehydrate the lower stratosphere in a significant manner because it makes the CPT colder, and air parcels generally travel for a couple of weeks near the CPT before they enter into the lower stratosphere (e.g., Fueglistaler et al., 2005).

The convectively driven tropopause cooling has been reported in many studies (in slightly different forms). Johnson and Kriete (1982) highlight the occurrence of a near-tropopause cold anomaly atop of deep convection using radiosonde observations over the western Pacific. Kiladis et al. (2001) showed that the cold anomaly is significantly correlated with convective activity on intraseasonal and interannual time scales using radiosonde and reanalysis data. Using Global Positioning System (GPS) radio occultation (RO) data, Randel et al. (2003) and Randel and Wu (2005) showed that vertical structure of the cold anomaly resembles that of the equatorial Kelvin waves. Paulik and Birner (2012) examined detailed characteristics of the cold anomaly by combining CloudSat radar measurements of deep convection and GPS RO temperature data and showed that the cold anomaly could last longer than a week, particularly related to tropical deep convection in boreal winter.

A relationship between the tropopause-level cooling and the Madden-Julian Oscillation (MJO) has also been reported in several studies. Zhou and Holton (2002) reported coherent eastward propagation of the tropopause-level cold anomaly with MJO convection using reanalysis data. They also showed that the anomaly is phase shifted with respect to MJO convection by about a quarter wavelength at the tropopause. Kim and Son (2012) have confirmed this phase relationship using GPS RO data, and Virts and Wallace (2014) further quantified the large-scale structure of the cooling and associated circulation pattern linked to the MJO using GPS RO and reanalysis data.

Although the convectively driven tropopause cooling is a known feature and may have a significant impact on SWV, its behavior in different locations and seasons have not been characterized, and detailed links to SWV are not fully understood. Therefore, understanding the behavior of the tropopause cooling and its links to water vapor are the main foci of this paper. In this study, we will investigate the characteristics and formation mechanism(s) of the tropopause cooling by extending the methodology used in Paulik and Birner (2012). Influences of the tropopause cooling on TTL moisture will also be examined and discussed. This paper is organized as follows. Data and method used in this study are described in section 2. The results are described in section 3 including the characteristics of sampled deep convection, the temperature responses in the TTL over the western Pacific and Asian monsoon region, and moisture response in the TTL. Dynamics of the tropopause-level cooling is discussed in section 4, and conclusions is given in section 5.

2. Data and Method

This study is based on composite analyses, utilizing temperature (from GPS RO), circulation (from reanalysis), and moisture (from Aura Microwave Limb Sounder; MLS) anomalies composited around cases of extreme deep convection obtained from CloudSat. Details of the data sets are described below.

2.1. Deep Convection Samples From CloudSat

Deep convection samples are obtained from the cloud classification product of CloudSat (2B-CLDCLASS; Sassen & Wang, 2008). CloudSat utilizes a millimeter wavelength radar (94 GHz), which is sensitive to condensates and precipitation in clouds, and provides detailed cloud information with a high vertical resolution (physical resolution is ~500 m; Stephens et al., 2002, 2008). CloudSat 2B-CLDCLASS data classify clouds into eight types using an algorithm based on horizontal and vertical structures of hydrometeor

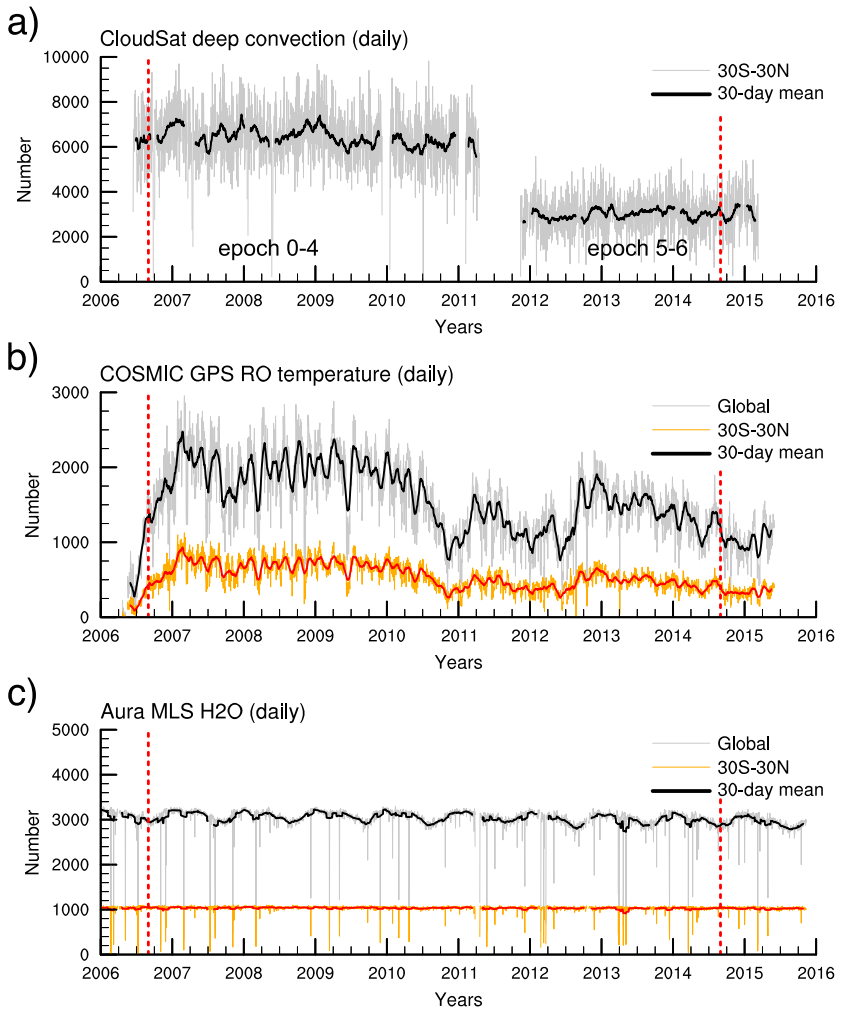

Figure 1. Daily count of (a) deep convection profiles sampled by CloudSat (2B-CLDCLASS) in the tropics (30°S–N), (b) temperature profiles observed by COSMIC GPS RO, and (c) water vapor from Aura MLS over the globe (thin gray) and over 30°S–N (thin orange). Thick curves show 30 day running average of the daily. Red vertical lines indicate period of data used for this study (September 2006 to August 2014).

and precipitation from radar reflectivity and background meteorological data. It reasonably isolates deep convection from trailing high clouds in a complex convective system (Sassen & Wang, 2008); thus, it is useful data for capturing overshooting convection. Only profiles classified as deep convection is used for this study. Due to its frequent sampling, horizontal resolution of the cloud sample is ~1 km along track. We define separate events of deep convection by connecting CloudSat samples located within 100 km along the orbit track. To avoid overlap between deep convection samples (i.e., sampling the same system multiple times), we further thin out the samples to have distance between separate events larger than 1,000 km. Among these data we focus on deep convection groups with maximum cloud top higher than 17 km. The selection method is utilized to avoid duplicated use of the dense along-track observations, and overall results are not sensitive to the selection criteria. One relevant aspect of the CloudSat sampling is that measurements are made near local times of 1:30 a.m. and 1:30 p.m. and hence probably undersample extreme convection over land where a large diurnal cycle occurs, with extreme convection in late afternoon (Liu & Zipser, 2008).

2.2. Temperature and Moisture Information From COSMIC GPS RO and Aura MLS

Temperature soundings are obtained from Constellation Observing System for Meteorology, Ionosphere, and Climate (COSMIC; Anthes et al. 2008) GPS RO measurements. The COSMIC mission provides ~1,600 temperature profiles (~400 profiles in the tropics) per day, with retrieved temperatures sampled on a 200 m vertical

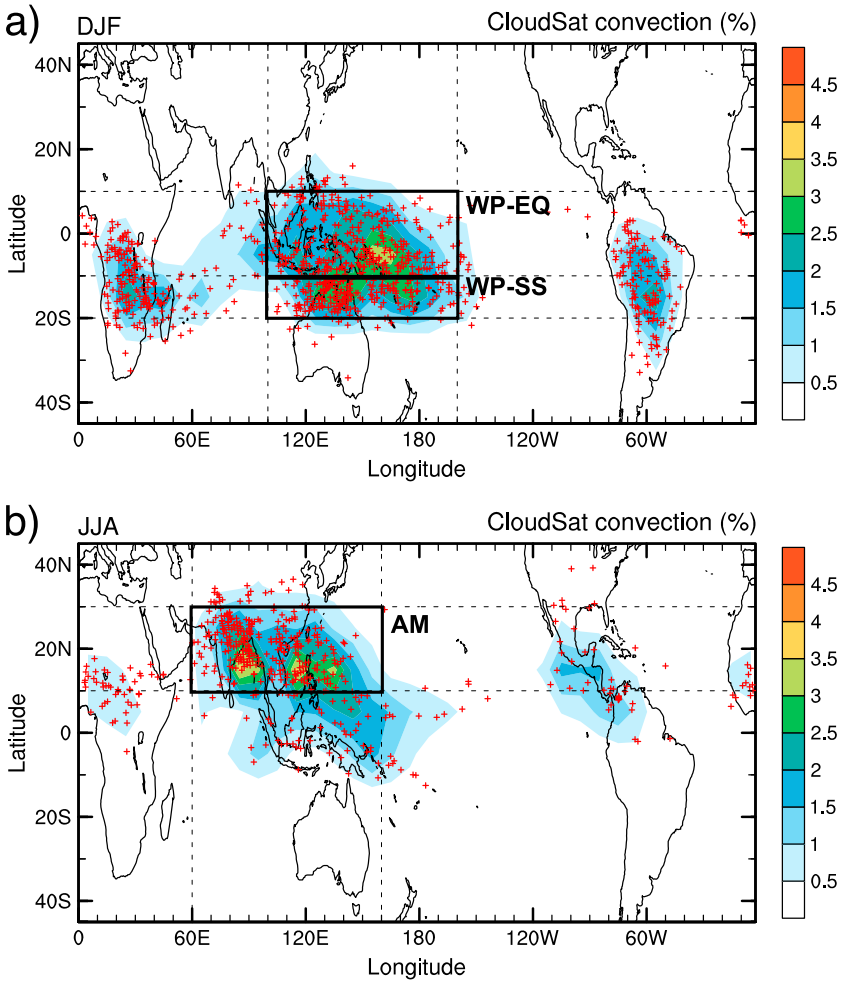

Figure 2. Spatial distribution of the tropical convection observed by CloudSat in (a) DJF and (b) JJA during September 2006 to August 2014. Frequency distribution of deep convection higher than 15 km is shown as shading (%), and extreme cases (cloud top height > 17 km) sampled for composite analysis (DC17) are shown as red crosses. The frequency of 15 km convection is computed as a number of 15 km deep convection divided by total number of observation in a given 10° × 10° grid box.

grid. The vertical resolution of GPS RO data is ~1 km in the upper troposphere and stratosphere, with a precision of ~0.25 K (Anthes et al., 2008; Kursinski et al., 1997), and it is known to accurately capture the temperature structure near the tropopause (e.g., Kim & Son, 2012). Water vapor data are obtained from the Microwave Limb Sounder (MLS) on board the Aura satellite, which is part of the A-Train constellation along with CloudSat. MLS provides water vapor profiles in the upper troposphere and stratosphere (above 13 km) with a vertical resolution of 3 km (Livesey et al., 2015).

2.3. Supplement-Gridded (Re)analyses

To complement the satellite observations, several gridded products are used. The Tropical Rainfall Measuring Mission (TRMM) Multisatellite Precipitation Analysis (TMPA; Huffman et al., 2007) is used to estimate rain rate (and associated latent heating) associated with deep convection identified by CloudSat. It provides 3-hourly rain rate on 0.25° × 0.25° horizontal grids incorporating multiple satellite measurements. Although TMPA is a satellite-based estimation of rain rate, it is known to capture large convective events successfully on subdaily time scale (Huffman et al., 2007). We also use the ERA-Interim reanalysis (Dee et al., 2011) zonal and meridional winds in order to examine circulation patterns in the TTL. The National Oceanic and Atmospheric Administration (NOAA) interpolated Outgoing Longwave Radiation (OLR; Liebmann & Smith, 1996) and OLR MJO index (OMI; Kiladis et al., 2014) are used to define MJO events.

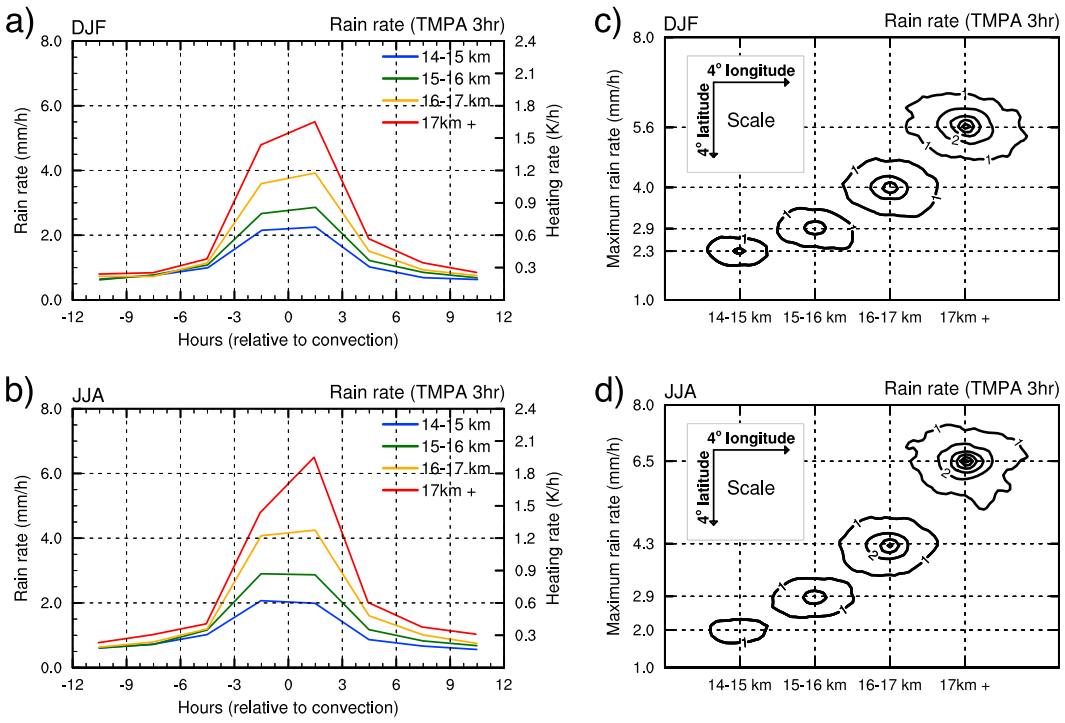

Figure 3. (a, b) Time series and (c, d) horizontal distributions of 3-hourly rain rate composited for different cloud top heights of deep convection sampled from CloudSat during (top) DJF and (bottom) JJA. Rain rates are obtained from 3-hourly TRMM Multisatellite Precipitation Analysis and composited with respect to the individual samples in space and time. Heating rates are estimated from rain rate by assuming uniform tropospheric latent heating (between 200 and 1,000 hPa). Contours are 1 mm/h, and horizontal scale is denoted in degree latitude/longitude.

2.4. Composite Method

Composite temperature and water vapor structures are calculated in coordinates relative to the identified deep convection, using a grid resolution of 10° longitude × 5° latitude. Specifically, for each CloudSat convection sample GPS RO temperature profiles are collected for 1 day (12 h before and after the deep convection). Temperature anomalies for each profile are computed by subtracting background profiles that are interpolated in space and time from an 8 year monthly climatology. Lastly, the temperature anomalies are averaged in the convection-relative grids. Thus, the temperature anomalies are presented in "relative longitude" and "relative latitude," in which convection is centered at zero longitude and latitude. MLS water vapor anomalies are calculated and averaged in the same manner, except that 3 days of measurements around each convection event are used to obtain enough samples in longitude.

The combined data sets used in this study are available from mid-2006 to present, as illustrated in Figure 1. The number of CloudSat observations falls after 2011 because of battery problem occurred in CloudSat; thus, only day-time samplings are available after this time. However, horizontal distribution and fractional occurrence of the deep convection measured by CloudSat remains similar before and after 2011. We performed the analyses using the 8 year record from September 2006 to August 2014. There are some missing months in CloudSat due to instrument problems (particularly in 2011), but most of data are commonly available during this period (Figure 1).

3. Results

3.1. Characteristics of the Sampled Deep Convection

Figure 2 shows the frequency of occurrence and spatial distribution of deep convection (cloud top >15 km) observed from CloudSat. The distribution agrees well with that of a climatology of deep convection based on OLR (not shown). In December–February (DJF), a large portion of deep convection is found in the western Pacific warm pool with fractional occurrence up to 3–4%. There are two secondary maxima over South America and Central Africa, although the fractions in these regions are likely underestimated by CloudSat

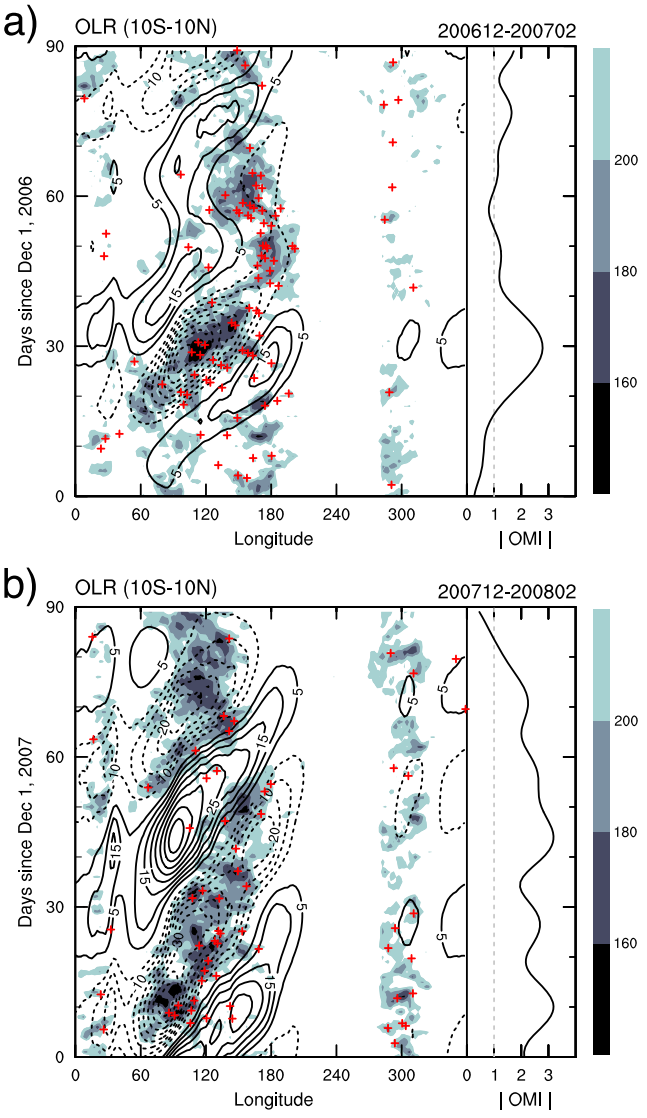

Figure 4. Longitude-time section of OLR (W m^{-2}; shading) and extreme convection samples (DC17, crosses) over 10°S–N during two boreal winters: (a) DJF 2006/2007 and (b) DJF 2007/2008. The OLR anomaly (W m^{-2}; contour) reproduced from the OLR MJO index (OMI) and amplitude of the OMI (right panels) are also shown.

sampling of the diurnal cycle, as noted above. In June-July-August (JJA) the convective activity is primarily concentrated over the Asian monsoon region. The sampled 17 km deep convection (red crosses in Figure 2, which will be referred as "DC17," hereafter) shows similar distributions with slightly more samples over north Australia in DJF and India in JJA. Fractional occurrence of 17 km convection is 0.1–0.3% over the western Pacific (maximum is found over north Australia) in DJF and 0.1–0.2% over India in JJA.

Figure 3 shows composites of 3-hourly TMPA rain rate composited with respect to colocated maximum cloud top heights. Overall, the rain rate is highly correlated with the maximum cloud top height. Figures 3c and 3d show that intensity and horizontal scale of the rain rate increase with higher cloud top of the convection, and similar behavior is found for samples during DJF and JJA. The maximum rain rate averaged for 17 km convection is ~5 mm/h (which is equivalent to diabatic heating of ~1.5 K/h assuming uniform heating by latent heat over 200–1,000 hPa), indicating release of strong latent heat at the center of the deep convection.

The region of significant rain rate spreads over several hundred kilometers in longitude and latitude in Figures 3c and 3d. The composite suggests that the sampled deep convection does not represent isolated thunderstorms but is part of organized convective systems (in agreement with Rossow & Pearl, 2007). DC17 are associated with large amounts of latent heat (several Kelvins per day) over a wide spatial range (hundreds of kilometers). These convection samples are of special interest because they represent potential overshooting deep convection that could directly transport water vapor (and ice particles) into the lower stratosphere. By using DC17, the behavior of overshooting convection is examined focusing on TTL temperature (sections 3.2 and 3.3) and moisture (section 3.4).

In this study, we focus on the western Pacific (WP) and Asian summer monsoon (AM) regions where the most active convection occurs in DJF and JJA, respectively. The western Pacific region is further divided into two parts by latitude (one region near the equator, WP-EQ; and the other in southern subtropics, WP-SS) because characteristics of temperature response are dependent on latitude. The regions are highlighted in Figure 2 (black boxes).

It is worth noting that deep convection over the western Pacific is often organized on large scales by the MJO. Figure 4 shows locations of DC17 within 10°N–S superimposed on daily OLR for two 90 day samples (DJF 2006–2007 and 2007–2008). The figure also shows the OLR anomaly filtered to highlight the MJO (Kiladis et al., 2014). There are clear overlaps between deep convection samples from CloudSat and low OLR anomalies, and most extreme convection samples are found in the active convective phase of the MJO. The relationship between DC17 samples and the MJO is summarized in Table 1. Over the western Pacific roughly 70% of samples are found during active MJO periods ($|OMI| > 1$) with slightly higher frequency in Phases 4 and 5, where MJO convection is found over the maritime continent. During boreal summer, convection over the Asian monsoon region is also affected by northward propagating MJO (or intraseasonal oscillation). Slightly, more convection samples are found during active phase of the summer-time MJO particularly during Phases 2, 3, 5 and 6.

3.2. Temperature Response Over the Western Pacific

As examples of individual events, two extreme convection cases during DJF are presented (Figure 5). Figure 5a illustrates a deep convective event over the maritime continent detected by CloudSat on 31 December 2006 (location is shown with red cross in OLR). Over this region, the OLR field shows a large

Table 1
Number of Extreme Convection Samples (Cloud Top Height > 17 km) Used in This Study

			MJO (|OMI| > 1)				
Region (season)	Total	No MJO |OMI| < 1	All	Phases 2 and 3	Phases 4 and 5	Phases 6 and 7	Phases 8 and 1
WP-EQ (DJF)	270	97	173	32 (18%)	60 (35%)	35 (20%)	46 (27%)
WP-SS (DJF)	201	51	150	23 (15%)	54 (36%)	40 (27%)	33 (22%)
AM (JJA)	282	123	159	50 (31%)	33 (21%)	54 (34%)	22 (14%)

Note. The samples are subdivided based on activity of the MJO using the amplitude of the OLR MJO index (OMI), and numbers in the parentheses show percentage for each phase.

envelope of high clouds with multiple OLR minima implying development of organized deep convection with multiple cores. The associated temperature anomaly indicates broad warming in the troposphere and a thin layer of near-tropopause cooling centered to the east of the deep convection. Another layer of warm anomalies is also observed in the lower stratosphere to the west of the convection, indicating a vertically tilted wave-like structure in the upper troposphere and lower stratosphere (UTLS). This temperature pattern is consistent with the structure of vertically propagating equatorial Kelvin waves. Such a pattern has been characterized in several previous studies, based on radiosonde data (Kiladis et al., 2001), GPS RO data (Kim & Son, 2012; Randel et al., 2003; Scherllin-Pirscher et al., 2017), reanalysis (Flannaghan & Fueglistaler, 2013), and idealized numerical modeling (Ryu et al., 2008).

However, the temperature anomalies do not always show a Kelvin-wave-like structure. Figure 5b presents another case associated with deep convection over the central Pacific. Although it shows a similar vertical dipole of temperature anomalies shifted to the east of the convection center, the anomalies do not exhibit a wave-like structure in the TTL.

The temperature response, particularly the tropopause-level cold anomaly, has been explained with two different hypotheses: a large-scale Kelvin wave response (e.g., Kiladis et al., 2001; Randel et al., 2003) and hydrostatic adjustment to convective heating (Holloway & Neelin, 2007). To examine the general

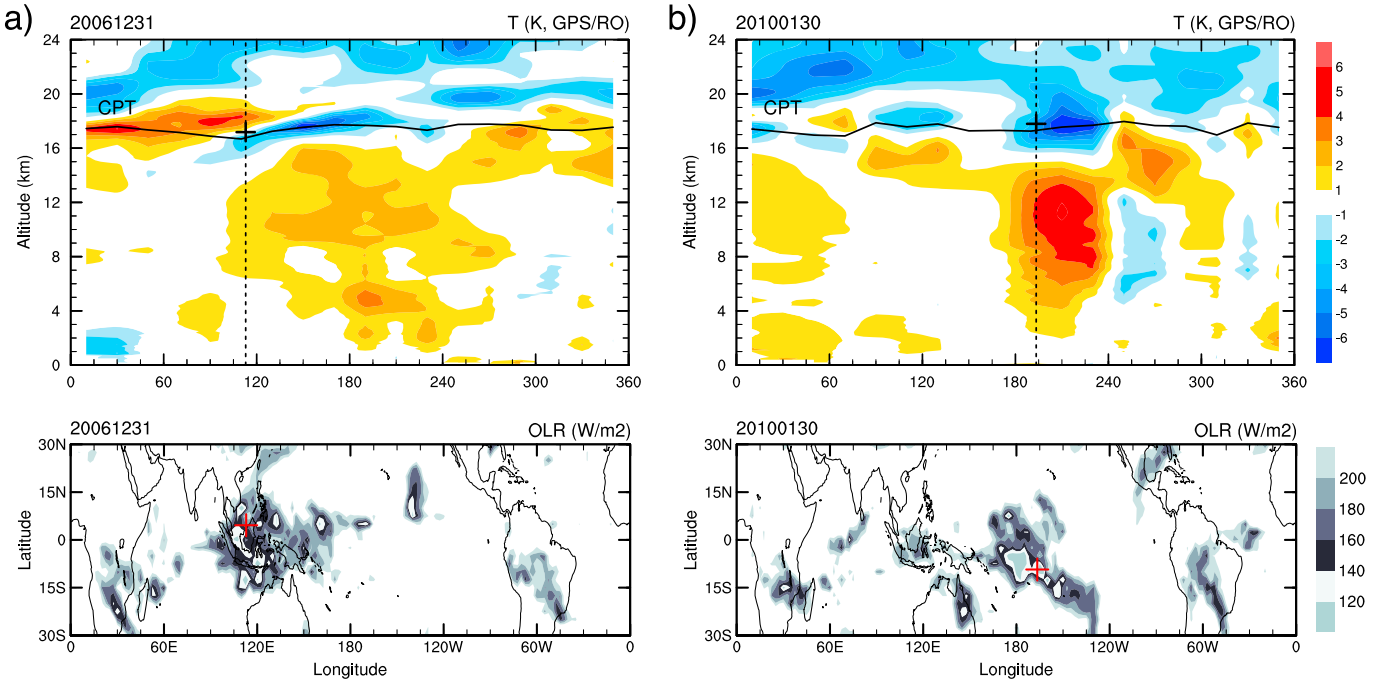

Figure 5. Longitude-altitude structure of the temperature anomaly from COSMIC GPS RO for extreme convection cases (cloud top height > 17 km) on (a) 31 January 2006 and (b) 30 January 2010. Bottom panels are outgoing longwave radiation on the same day. Crosses indicate location and maximum cloud top height of the deep convection, and black horizontal lines denote the cold point tropopause.

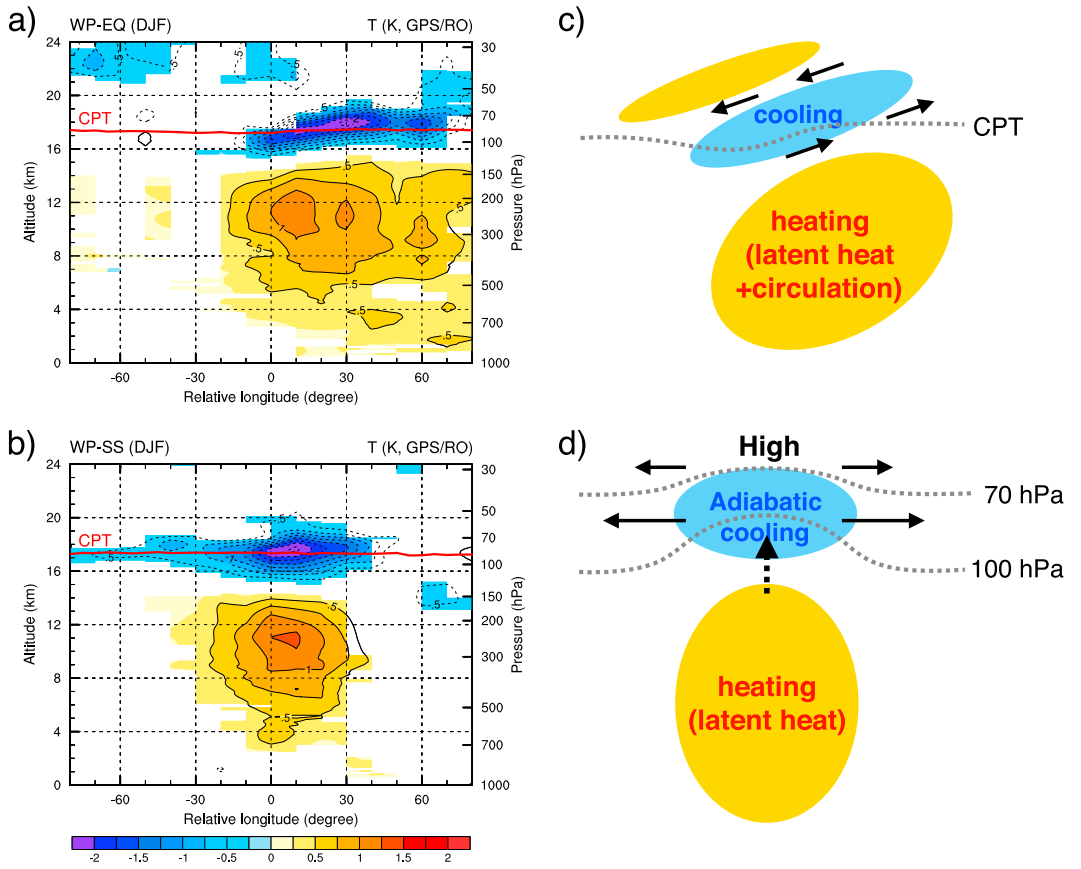

Figure 6. Longitude-altitude structure of temperature anomalies from COSMIC GPS RO composited for extreme convection (cloud top height > 17 km; DC17) over (a) WP-EQ and (b) WP-SS in DJF, and schematic diagrams of (c) Kelvin waves and (d) hydrostatic adjustment. The abscissa represents relative longitude with respect to the location of convection. Contour intervals are 0.25 K, and 0, ±0.25 contours are omitted for visual clarity. Shading indicates significant values at 95% confidence level. Red horizontal lines denote the cold point tropopause.

characteristics of the temperature response, we produce composite temperature anomalies for WP-EQ (Figure 6a) and WP-SS (Figure 6b). The 270 deep convection samples are used for WP-EQ, and 201 samples are used for WP-SS. On average one or two temperature profiles are included in a grid box per one deep convection sample; thus, roughly 240 to 450 temperature profiles are averaged for a grid box. The composite temperature anomaly for WP-EQ is qualitatively similar to that of the example shown in Figure 5a. A clear vertical dipole of warm and cold anomalies appears to the east of the sampled deep convection. Although no additional warm anomaly appears in the lower stratosphere, the cold anomaly in the TTL shows an eastward phase tilt with height consistent with a Kelvin wave response, which is schematically described in Figure 6c. For WP-SS, the temperature anomaly shows also a dipole structure, but no vertical tilt is observed, and its center is more aligned with the location of the deep convection compared to WP-EQ. The difference in vertical structure is not surprising because the Kelvin wave response is expected only near the equator. This pattern is similar to that in Figure 5d and is consistent with the hydrostatic adjustment structure described in Holloway and Neelin (2007) that is schematically depicted in Figure 6d. The in-phase vertical structure is a characteristic of hydrostatic adjustment, and it stands out even more clearly when compositing only over the 15–20°S latitude band (not shown).

In fact, the contributing mechanism can be clarified by using a relationship between temperature and pressure anomalies. In a pure Kelvin wave, these anomalies have a quadrature relationship where "high pressure" leads "cold anomaly," while they have an in-phase relationship in pure hydrostatic adjustment. Our analysis (based on reanalysis meteorological data, not shown) suggests that both mechanisms contribute to the tropopause cooling over WP-EQ, while hydrostatic adjustment dominates over WP-SS and the ASM.

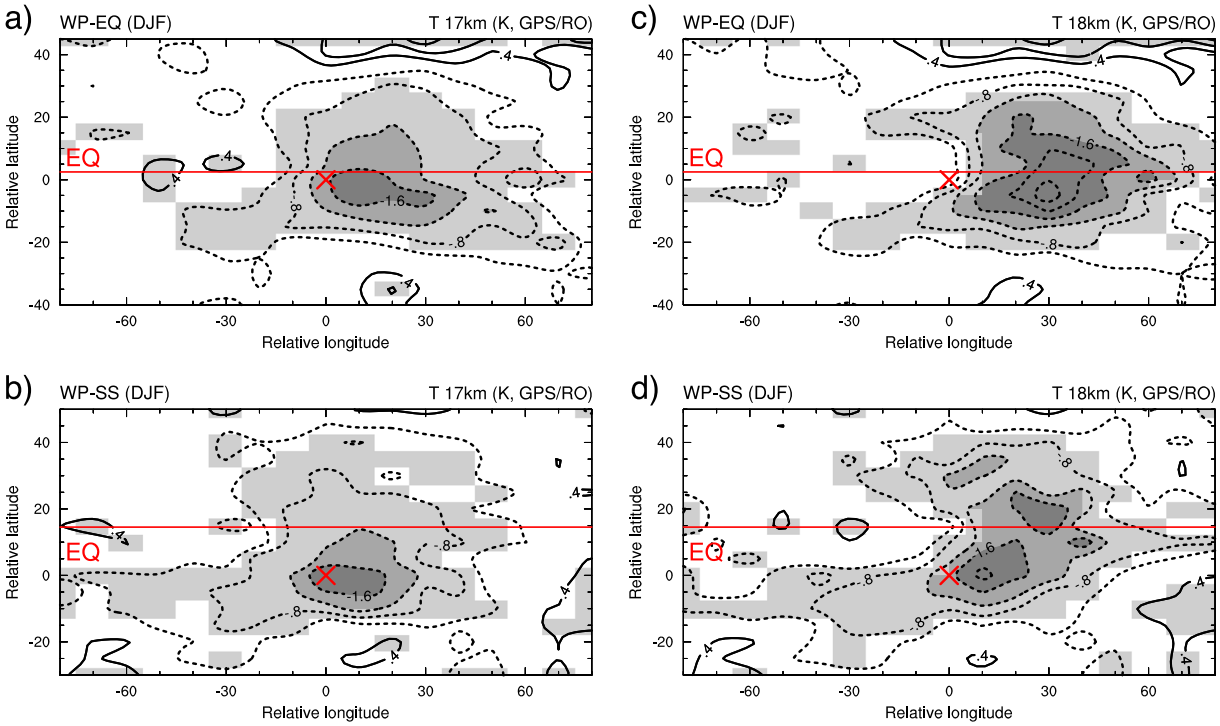

Figure 7. Horizontal structure of the cold anomaly at 17 (left panels) and 18 km (right panels) composited for extreme convection (cloud top height > 17 km; DC17) over (a, c) WP-EQ and (b, d) WP-SS. Significant values at 95% confidence level are shaded. Red crosses indicate location of the sampled convection, and red horizontal line denotes mean location of the equator.

The eastward shifted temperature response over WP-EQ is an interesting feature. It has been reported by several studies focused on the TTL (e.g., Kim & Son, 2012; Virts & Wallace, 2014; Zhou & Holton, 2002) and troposphere (e.g., Hendon & Salby, 1994). The shifted temperature anomalies are likely related to a Kelvin wave response to a diabatic heating, where large-scale circulations redistribute the heat by interacting with convection (Hendon & Salby, 1996).

Figure 7 presents the horizontal structure of the cold anomaly at 17 and 18 km where the strongest cooling is found. The cold anomaly is generally confined to within ±20° from the Equator covering several tens of

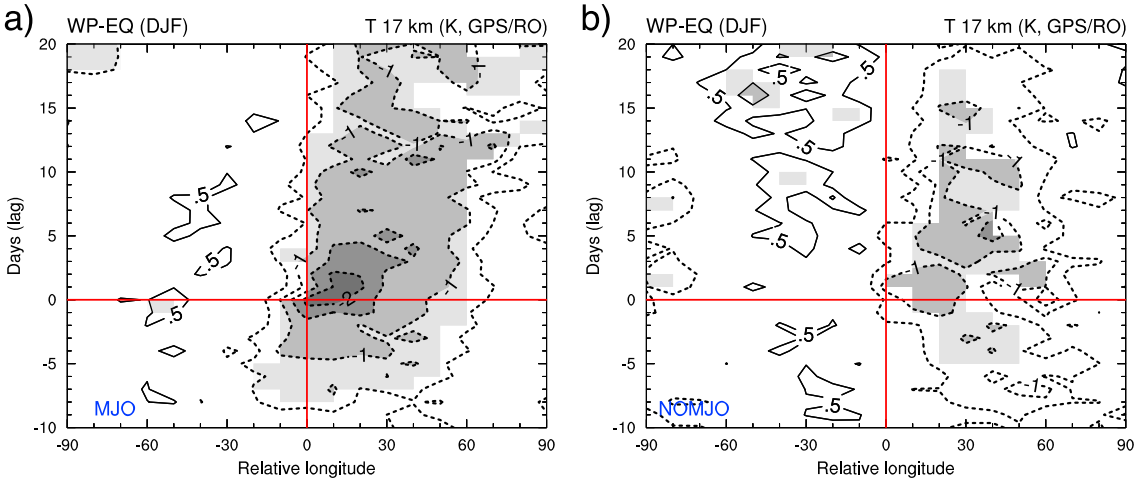

Figure 8. Longitude-time section of the cold anomaly at 17 km. Temperature anomalies are obtained in the same way as in Figure 4 with time lags (in days) for MJO (left panels) and non-MJO (right panels) cases over WP-EQ. Contour interval is 0.5 K, and significant values are shaded with 95% confidence level.

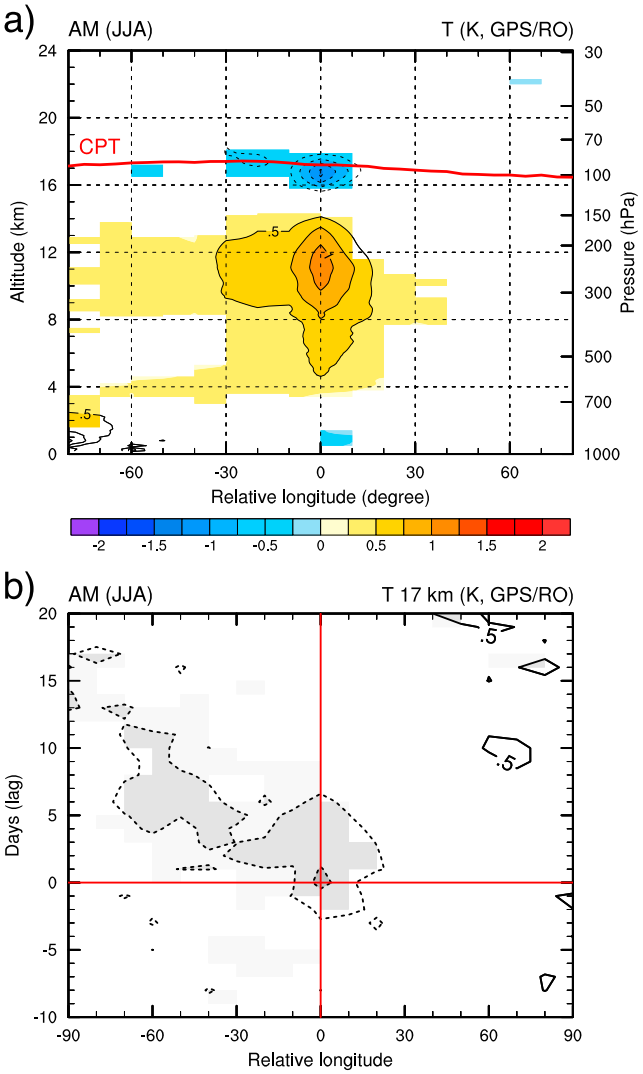

Figure 9. (a) Composited temperature anomalies for extreme convection (cloud top height > 17 km) over AM in JJA. The longitude-time section (b) shows temperature anomaly at 17 km, where maximum amplitude of cold anomaly appears. Contour intervals are 0.25 K (0, ±0.25 contours are omitted) for upper panel, and 0.5 K for lower panel.

degrees in latitude and longitude. The latitudinal scale matches roughly that of equatorially trapped waves, which is determined by the equatorial Rossby radius of deformation.

The horizontal structure of the cooling is quite symmetric around the averaged location of the equator for WP-EQ (Figures 7a and 7c), and even for WP-SS (Figures 7b and 7d) except for a slightly stronger anomaly found near the center of the deep convection. Particularly, the temperature anomaly at 18 km resembles a "horseshoe"-shaped Matsuno-Gill-type response (Gill, 1980) as discussed in several previous studies (e.g., Highwood & Hoskins, 1998; Kiladis et al., 2001; Nishimoto & Shiotani, 2012). Although the temperature anomalies over WP-EQ and WP-SS show different vertical structures in Figure 6, they are likely a part of a Matuno-Gill-type response to a broad tropical heating. The anomalies over WP-EQ belong to Kelvin-wave part, and the anomalies in the WP-SS belong to Rossby-Wave gyre in a Matuno-Gill-type response. This is likely due to the fact that a large portion of the extreme convection samples are related to organized convection in the MJO as seen in Table 1.

One noticeable feature of the tropopause-level cooling is its horizontal scale. It covers ~6,000 km in longitude with a maximum amplitude of −2 K, consistent with the results in Paulik and Birner (2012). The temperature minimum is located near the CPT implying that ~1–2 K of additional cooling appears at the CPT over a wide range of longitudes when extreme deep convection occurs over the western Pacific. Thus, the tropopause cooling could significantly enhance the freeze-drying process, particularly when its lifetime is comparably large to transport time scale in the TTL.

The temporal behavior of the tropopause-level cold anomaly is shown in Figure 8. Because convection in the MJO shows a characteristic behavior, the composite is made separately for MJO and non-MJO (or weak MJO) periods based on the classification in Table 1. During an active MJO period, a significant cold anomaly is found roughly a week before the sampled extreme convection for WP-EQ (Figure 8a). It is found ~10–20° east of the convection and moves slowly to the east over time. The same behavior is also found for WP-SS (not shown). This propagation and time scale is consistent with the movement of the MJO (Figure 4). The temperature anomalies therefore follow the MJO envelope persisting for several weeks. The temperature composite during non-MJO period, on the other hand, shows a notably weaker anomaly lasting roughly 1 or 2 weeks. This large difference between MJO and non-MJO cases is also clearly shown in the vertical structure of the temperature anomalies (supporting information Figure S1). This suggests that a well-organized convective system (such as MJO) acts to amplify and maintain the tropopause-level cooling for several weeks.

The overall features of the cold anomaly over the western Pacific suggest that the cooling effect in the TTL is not due to a single convective tower, but it is driven by an interaction of a series of mesoscale deep convection and large-scale circulations embedded in the MJO. Although we cannot isolate the influence of single overshooting convection on the tropopause temperature, this is likely a general feature of the tropopause-level cooling observed over the western Pacific because deep convection occurs mostly in a well-organized convective system in this region (Rossow & Pearl, 2007).

3.3. Temperature Response in the Asian Monsoon Region

Composite analysis was also constructed for the Asian monsoon region during JJA (Figure 2b). The temperature composite over AM (Figure 9a) shows a similar dipole pattern of warm (in the troposphere) and cold (at

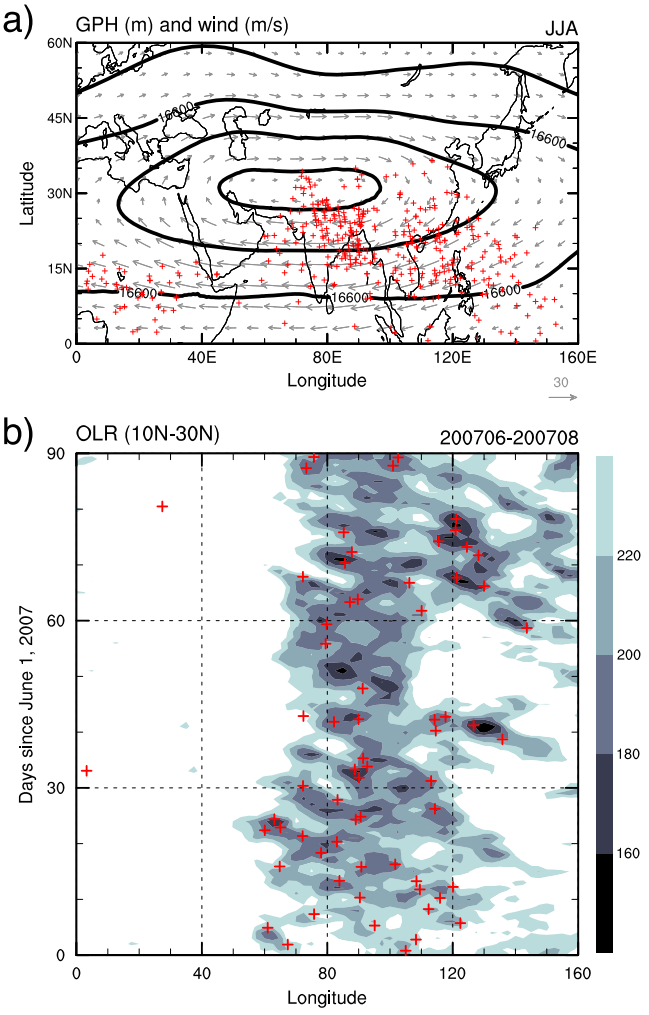

Figure 10. (a) Geopotential height (m, contour) and wind (m s^{-1}, vector) at 100 hPa superimposed with extreme convection samples (DC17, crosses). (b) Longitude-time section of OLR (W m^{-2}; shading) and extreme convection samples (DC17, crosses) over 10–30°N during JJA 2007.

tropopause) anomalies. However, the horizontal scale and the strength of the anomalies are significantly smaller compared to those over the western Pacific. This is consistent with Paulik and Birner (2012), who quantified the different responses during JJA versus DJF. A large number of convection samples during JJA are over the Asian monsoon region in their study, and Figure 9a is virtually the same with their JJA temperature response.

The cold anomaly near the AM CPT has a lifetime of ~10 days, with an amplitude of ~ −0.5 K, that is, weaker than that of WP-EQ. It moves westward from the center of the convection sample over time, with a speed of ~5°/d (Figure 9b). This behavior is likely due to propagation characteristics of the monsoon disturbances, which are known to propagate northwestward (Lau & Lau, 1990), and partly a westward drift of the convective systems by large-scale monsoon circulation. Most of the sampled deep convection occurs in the southern part of the Asian monsoon anticyclone (Figure 10a) where the background winds are easterly. The OLR evolution (Figure 10b) confirms the westward movement of major convection systems in this region.

The temperature anomalies are much weaker and smaller over the Asian monsoon region compared to that in the western Pacific, even though the averaged rain rate (latent heating) associated with the sampled convection in both regions are comparable in magnitude and spatial scale (see Figure 2). This contrast may be related to different characteristics of convective activity over the two regions. OLR over AM exhibits a nearly continuous evolution of active convection (Figure 10b), while deep convection often shows large spatial and temporal variations in the WP-EQ related to phase of the MJO. Furthermore, the cold anomaly once formed in the AM region could remain as a quasi-stationary response through geostrophic balance (within the time scale of the beta drift and friction), while the cold anomaly in the deep tropics is rather a transient response. This implies that the seasonal climatology of temperature over AM already has a strong convective cooling signature near the tropopause, and temperature anomaly to DC17 could be underestimated with this background climatology. These are possible explanations for the weak temperature response in the AM region, but we could not clearly understand the reason.

3.4. Moisture Response in the TTL

The observed cold anomaly is expected to have a significant influence on the moisture content in the TTL—this influence is examined focusing on the western Pacific regions. Figure 11a shows the vertical structure of the composite water vapor for extreme convection over WP-EQ during active MJO periods as observed by Aura MLS. Despite the coarser vertical resolution of MLS, the corresponding water vapor anomalies in this region show a very similar vertical structure with the temperature anomalies (compare with Figure 6a). In particular, a clear dry anomaly is found where the cold anomaly is located in the TTL with a slight eastward tilt with height. This strong coherence between the water vapor and temperature fields suggests that dehydration through the freeze-drying is enhanced by additional cooling in the TTL by deep convection.

A significant dry anomaly is also found in the middle-to-lower TTL to the west of the deep convection, where temperature anomalies are small. Transport of dry air from the east is possibly responsible for this dry anomaly. In order to check this possibility, the same composite analyses are conducted for zonal wind from ERA-Interim reanalysis and ozone from MLS data (the results are provided as supporting information, Figure S2, to focus on temperature and water vapor in the main text). The composite of zonal wind shows anomalous easterlies in the TTL and likely helps to transport the dry air in the cold anomaly to the further west. The composite of ozone presents a similar structure supporting the idea of transport impact in the TTL. Particularly, a

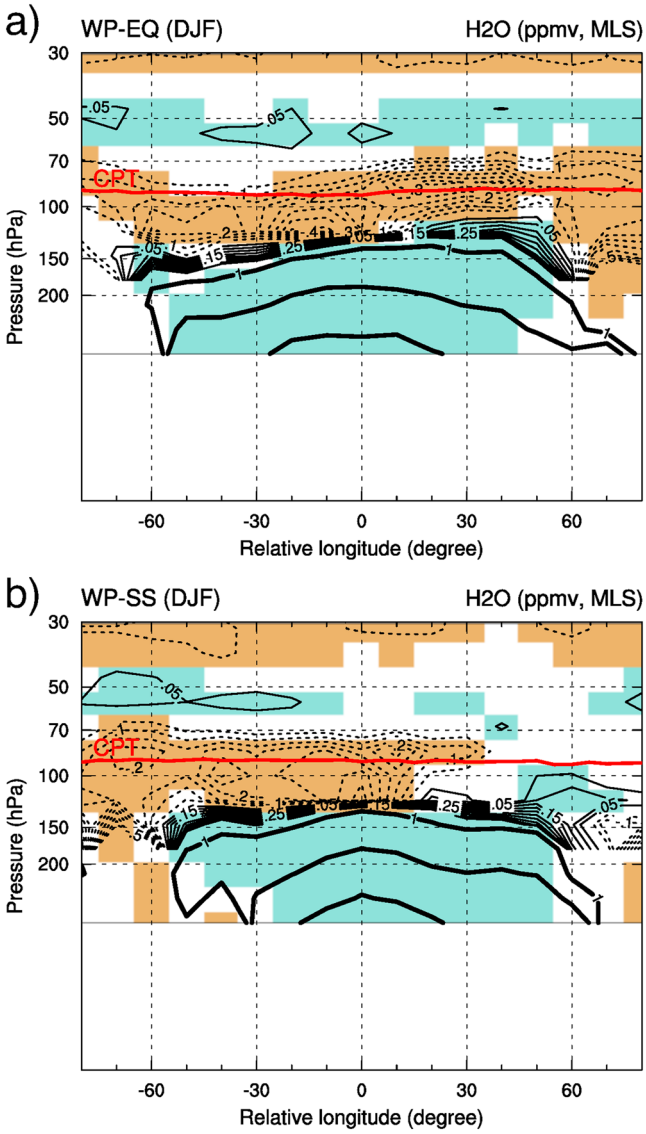

Figure 11. Longitude-altitude structure of water vapor anomalies from Aura MLS (ppmv, contour) composited for extreme convection during active MJO periods over (a) WP-EQ and (b) WP-SS. Significant values at 95% confidence level are shaded. Contour interval is 0.05 for thin lines, and 1, 10, and 100 ppmv values are denoted by thick lines.

strong negative ozone anomaly is found in the cold anomaly. This negative ozone anomaly implies a transport of ozone-poor air from the troposphere along the slope in this region (this could be thought like a transport of air mass with low potential temperature). The role of transport will be further examined in the later part of this section.

The water vapor anomalies over WP-SS (Figure 11b) show dry patterns in the TTL, although the anomalies are spread out mostly to the west of the cold anomaly centered on the deep convection region (Figure 6b). This behavior can be better understood from the corresponding horizontal structure; Figure 12 shows composite water vapor anomalies at 83 hPa for WP-EQ and WP-SS. The spatial structure of dry anomalies is virtually the same as that of the cold anomaly (Figure 7) for both WP-EQ and WP-SS. The dry anomalies in both regions exhibit a symmetric pattern along the equator with the maximum dryness at the equator. These coherent spatial patterns highlight the strong control of temperature on water vapor in the TTL.

In addition to the temperature control, the water vapor structure could be locally modified by transport. The streamlines in Figure 12 show the composite of horizontal circulation structure in the TTL for DC17 samples during active MJO periods. The off-equatorial branches of the dry anomaly coincide well with the outflow from the dry region. This implies that transport by the anomalous circulation driven by deep convection also contributes to redistribution of the dry anomalies in the TTL. A further analysis on time-lagged composite of the moisture anomaly (supporting information Figure S3) demonstrates that the dry region expands along the anomalous circulation over time, supporting this interpretation. A similar dehydration mechanism was proposed by Takashima et al. (2010) for a minimum SWV event.

Figure 13a shows the time evolution of the dry anomaly at 83 hPa for WP-EQ during active MJO. The evolution of the dry anomaly at 83 hPa closely follows the behavior of the cold anomaly at 17 km (Figure 8). It propagates slowly to the east following the cold anomaly over time, while further spread of dry signal is found after ~10 days. The dry anomaly of WP-SS shows fundamentally the same behavior (not shown) as in WP-EQ. The horizontal spread of dry signal is largely due to the effect of circulation pattern found in Figure 12, which is clearly shown in the time evolution of the dry anomaly (Figure 13a and supporting information Figure S3). The role of large-scale circulation response in dehydration process of the TTL has been discussed in Hatsushika and Yamazaki (2003) and Fueglistaler et al. (2005). This observational result clearly manifests the detailed process discussed in previous studies.

It is worth to note that a composite for extreme convection sampled during non-MJO (or weak MJO) periods show no clear dehydration or hydration signal (Figure 13b). In the western Pacific, the MJO is likely the most important convective activity that affects moisture in the TTL. This results emphasize the role of organized deep convection on dehydration process in the TTL, which is discussed in Randel et al. (2015) and Virts and Houze (2015).

The temperature and circulation responses observed over the western Pacific could be understood as a Matsuno-Gill-type response (Highwood & Hoskins, 1998) to transient convective heating related to the MJO (Kiladis et al., 2001; detailed upper-level circulation pattern is also available at NOAA Earth System Research Laboratory MJO Web page, https://www.esrl.noaa.gov/psd/mjo/mjoindex/pdf/psi200.1x.20ns.omi.amp1.096.djf.7912.pdf). The equatorial part is explained as the Kelvin wave component, and the

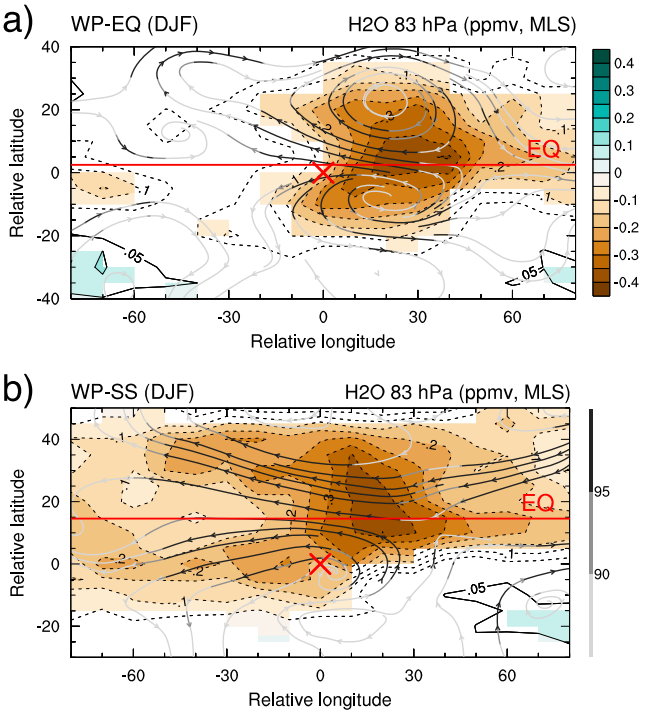

Figure 12. Horizontal structure of water vapor anomaly (ppmv) at 83 hPa measured from Aura MLS and 70–100 hPa circulation anomalies (streamline) composited for extreme convection (DC17) over (a) WP-EQ and (b) WP-SS occurs during active MJO periods. Significant values of water vapor at 95% confidence level are shaded (color bar in the upper panel), and the streamlines are colored by significant levels (color bar in the lower panel). Red crosses indicate the location of extreme convection, and red horizontal line denotes mean location of the equator.

off-equatorial part is explained with the Rossby wave component. Particularly, the off-equatorial part evolves into two isolated anticyclones centered at ~15°N and 15°S over time(Figure 14a). The same pattern is found in temperature (Figure 14b) and water vapor anomalies (Figure 14c), and this structure is reminiscent of the dehydration pattern shown in Schoeberl and Dessler (2011; in their Figure 9a).

4. Dynamical Balances for the Tropopause-Level Cooling

One interesting feature of the tropopause cooling is its small vertical depth (~3 km) compared to that of its tropospheric counterpart (~10 km). The different vertical scales of the cold and warm anomalies may be explained by differences in background buoyancy frequency, N. Because meridional scale (L^y) of the cold and warm anomalies are coupled through hydrostatic balance, that is, $L^y_{\mathrm{cold}} = L^y_{\mathrm{warm}}$ (the subscripts "cold" and "warm" refer to properties of the cold and warm anomalies), assuming that the meridional scale of the anomalies follows the equatorial Rossby radius of deformation, $R_d = \sqrt{N/\beta m}$ (where N is static stability, β is meridional gradient of Coriolis parameter, and m is vertical wave number), we can get $\sqrt{N_{\mathrm{cold}}/\beta m_{\mathrm{cold}}} = \sqrt{N_{\mathrm{warm}}/\beta m_{\mathrm{warm}}}$, and which gives

$$L^z_{\mathrm{cold}} = \left(\frac{N_{\mathrm{warm}}}{N_{\mathrm{cold}}}\right) L^z_{\mathrm{warm}}$$

(where L^z is the vertical scale of the anomaly, which is $2\pi/m$). Thus large static stability in the background leads to a vertically narrow temperature response. The vertical depth of the warm anomaly is likely determined by diabatic heating in the troposphere, and the observed ratio of N_{cold} (near the tropopause) versus N_{warm} (in the troposphere), which is ~3, explains the observed ratio between vertical depths of the warm and cold anomalies.

In addition, the vertical depth of the cooling determines its magnitude. In a balanced situation, the increase in geopotential height associated with the warm tropospheric anomaly should be compensated by decrease in thickness in the cold anomaly. Using hydrostatic balance ($d\Phi'/dz^* = RT'/H$, where Φ' and T' are geopotential

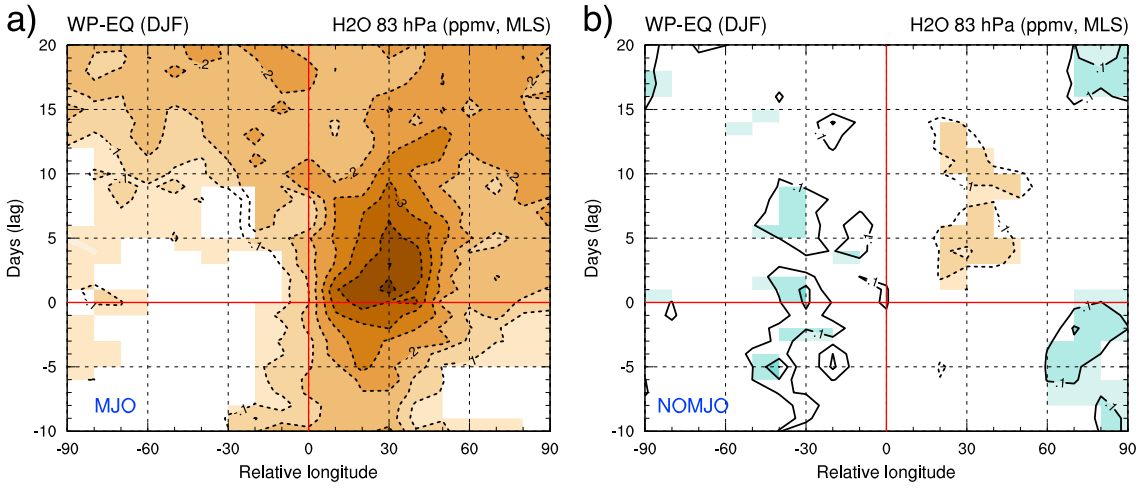

Figure 13. Longitude-time section of equatorial water vapor anomaly at 83 hPa for extreme deep convection (DC17) over WP-EQ during (a) active MJO and (b) non-MJO periods. Contour interval is 0.05 (±0.05 contours are neglected for visual clarity), and significant values are shaded at 95% confidence level.

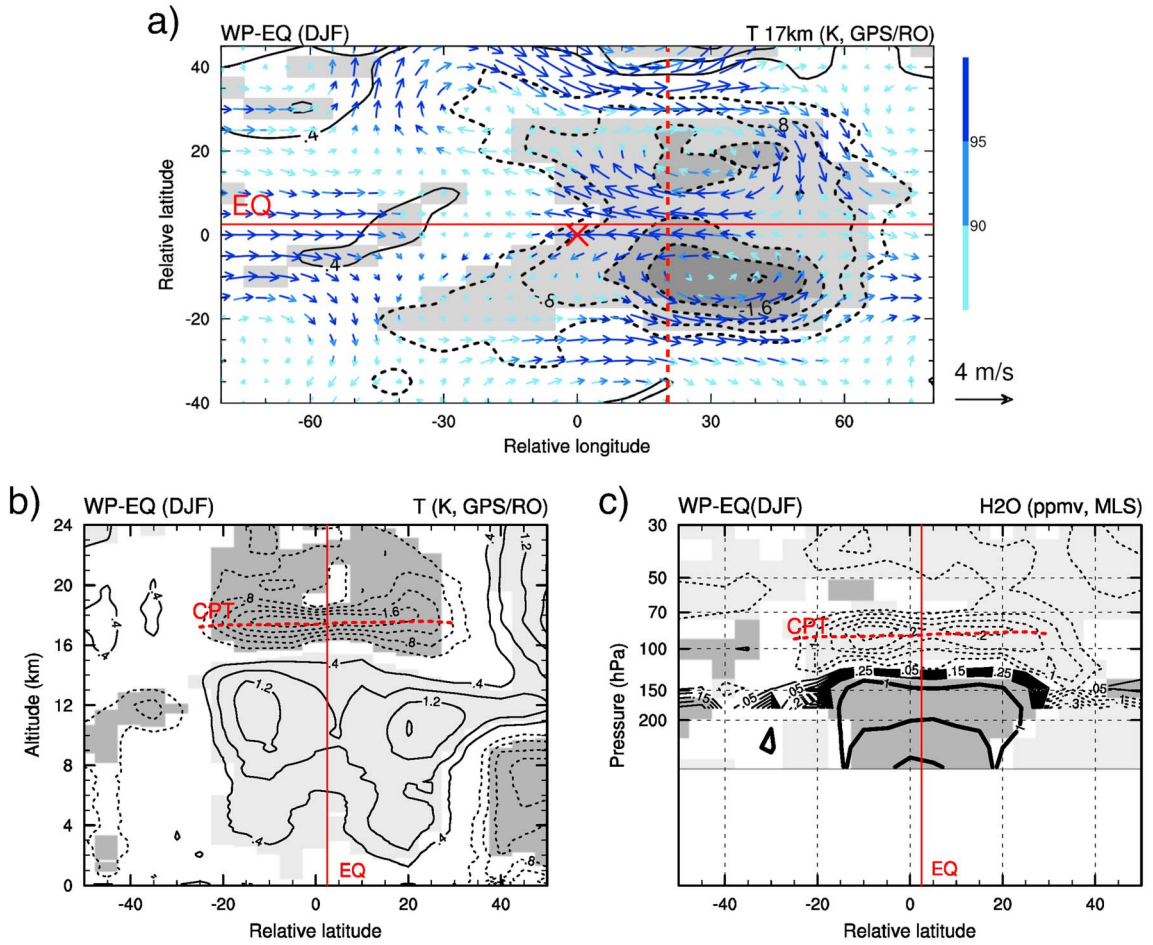

Figure 14. (a) Horizontal structure of 17 km temperature (contour) and 70–100 hPa wind anomalies (vector) obtained from 7 day lagged composite for extreme deep convection (DC17) over WP-EQ. Latitude-altitude structure of (b) temperature and (c) water vapor anomalies at 20° in relative longitude (denoted in dotted line in Figure 14a). Contour interval is 0.4 and 0.05 for temperature moisture anomalies, respectively. Significant values are shaded, and color of the vector denotes confidence level. Solid red lines denote mean location of the equator.

and temperature anomalies, z^* is log-pressure height, R is gas constant, and H is scale height), the relationship could be expressed as $\int T'_{\text{cold}} dz^*_{\text{cold}} = -\int T'_{\text{warm}} dz^*_{\text{warm}}$ (the integrations are made over the depths of cold and warm anomalies, respectively), that is, the magnitudes of warm and cold anomalies are inversely proportional to their depth scale. This explains why the intensity of the cold anomaly is ~3 times stronger than it tropospheric counterpart.

5. Conclusion

Large-scale temperature and moisture responses to extreme deep convection have been examined in the TTL for the highest clouds observed by CloudSat. Over the western Pacific during DJF, strong convection is mostly embedded in organized convective systems, and a large portion of deep convection samples (with cloud top >17 km) were found within the envelope of active MJO (Figure 4). The temperature response associated with the deep convection shows a clear vertical dipole structure of warming in the troposphere and cooling near the tropopause. In particular, the cold anomaly near the tropopause shows a distinct layered structure spreading along the CPT covering several thousand kilometers horizontally in the TTL. In composite analysis, it has average amplitude of ~ −2 K and lasts approximately 2–3 weeks, particularly with support of the MJO.

The moisture response is largely coherent in space and time with the temperature anomalies in the TTL. A large-scale dry anomaly is found associated with the tropopause cold anomaly. The dry anomaly further

expands along the outflow from the dry region on weekly time scales. The anomalous circulation response associated with deep convection is likely spreading the dry air from the cooling region in the TTL. This circulation anomaly shows coherent patterns with the temperature and moisture anomalies and is at least partly associated with the transient equatorial wave response to latent heating below. The overall dehydration process occurs effectively during active MJO periods, but no clear hydration or dehydration signal is found during weak- or non-MJO periods.

Our composite analyses based on multiple satellite observations show that the convectively driven tropopause-level cooling contributes significantly to dehydration in the upper TTL, particularly over the western Pacific. This is consistent with Randel et al. (2015) who found stratospheric dehydration subsequent to enhanced deep convection over the Asian and North American monsoon regions. The deep convection samples used in this study (cloud top $>$17 km) likely include overshoots and in principle allow direct transport of water vapor into the upper TTL and lower stratosphere, but such a signal does not appear to be strong enough to show up in the composite structures examined here. The method used in this study may be limited as it captures mostly large-scale averaged responses and could miss localized small-scale convective injection. However, the tropopause cooling and associated dry anomaly are robust features found over a wide area in the TTL when extreme deep convection occurs in the western Pacific. This suggests that the dominant impact of deep convection on the TTL is cooling and enhanced dehydration, at least for the western Pacific region.

The dehydration process discussed in this study is different from that proposed by Danielsen (1993) and Sherwood and Dessler (2000). They hypothesized that overshooting convection could dehydrate the lower stratosphere by direct injection of extremely cold air, ice formation, and subsequent sedimentation. The cold anomaly observed in this study is rather related to large-scale wave (or balanced) motions induced by an underlying heat source, and it exhibits a much larger horizontal scale compared to that of individual overshooting convection. The cold anomaly has also sufficiently long lifetime to allow ice particle sedimentation, which is important for efficient dehydration (Holton & Gettelman, 2001). This behavior is consistent with the recent study of Virts and Wallace (2014), which shows enhanced cirrus occurrence in conjunction with cold TTL temperatures and low water vapor during the MJO, based on Cloud-Aerosol Lidar and Infrared Pathfinder Satellite Observations data. Given the large horizontal scale and long lifetime, the dynamically induced tropopause cooling is expected to have a significant impact on stratospheric moisture.

Our composite analysis for extreme convection in the Asian monsoon region did not find clear dehydration (or hydration) signatures, but this may in part be related to the weak and confined temperature anomaly in this region (Figure 9a). The moisture response may also be sensitive to the location of the deep convection as hydration or dehydration is expected to be sensitive to the background relative humidity (specifically, the degree of subsaturation versus supersaturation, e.g., Jensen et al., 2007). Additionally, dehydration in the AM primarily occurs on the (cold) south side of the anticyclone, tied to the balanced response to organized large-scale (nonlocal) convection (Randel et al., 2015). Thus, spatial location of the deep convection may also be an important factor for the dehydration.

One hypothesis is that the large-scale temperature structure near the tropopause in the AM is mainly controlled by quasi-geostrophic dynamics associated with the anticyclonic circulation and upward bulging of tropopause-level potential temperature surfaces, which are maintained by a secondary circulation (Hoskins et al., 1985). Although the deep convective heating serves as the ultimate cause of the primary anticyclonic circulation, the secondary circulation is important because it balances the anticyclonic circulation with the underlying convective heating and the upper level temperature response. In this system, enhanced local convection can cause tropopause-level cooling only when it affects the large-scale balance of anticyclonic circulation in the AM. Therefore, a broad convection can effectively change the tropopause-level temperature rather than a localized overshooting convection.

Acknowledgments
The CloudSat cloud classification product, 2B-CLDCLASS, is obtained from CSU/CIRA CloudSat data server (http://www.cloudsat.cira.colostate.edu/). COSMIC GPS RO data are downloaded from UCAR CDAAC (at http://www.cosmic.ucar.edu/), and MLS and TMPA data are obtained from NASA GES DISC webpage (https://daac.gsfc.nasa.gov/). The NOAA OLR and OMI index were provided by the NOAA/OAR/ESRL PSD via their website (http://www.esrl.noaa.gov/psd/). We appreciate these institutions for making the data freely available for scientific research. We are also grateful to three anonymous reviewers for their constructive comments and suggestions. It helped much to improve the manuscript. This work was supported by the NASA GNSS Remote Sensing and Aura Science Teams. Joowan Kim is also partly supported by Basic Science Research Program through the National Research Foundation of Korea (NRF) funded by the Ministry of Science, ICT and Future Planning (2017R1C1B1009965).

References

Anthes, R. A., Ector, D., Hunt, D. C., Kuo, Y. H., Rocken, C., Schreiner, W. S., … Yen, N. L. (2008). The COSMIC/FORMOSAT-3 mission: Early results. *Bulletin of the American Meteorological Society*, *89*(3), 313–333. https://doi.org/10.1175/BAMS-89-3-313

Corti, T., Luo, B. P., de Reus, M., Brunner, D., Cairo, F., Mahoney, M. J., … Peter, T. (2008). Unprecedented evidence for deep convection hydrating the tropical stratosphere. *Geophysical Research Letters*, *35*, L10810. https://doi.org/10.1029/2008GL033641

Danielsen, E. F. (1993). In situ evidence of rapid, vertical, irreversible transport of lower tropospheric air into the lower tropical stratosphere by convective cloud turrets and by larger-scale upwelling in tropical cyclones. *Journal of Geophysical Research*, *98*(D5), 8665–8681. https://doi.org/10.1029/92JD02954

Dee, D. P., Uppala, S. M., Simmons, A. J., Berrisford, P., Poli, P., Kobayashi, S., … Vitart, F. (2011). The ERA-Interim reanalysis: Configuration and performance of the data assimilation system. *Quarterly Journal of the Royal Meteorological Society*, *137*, 553–597. https://doi.org/10.1002/qj.828

Dlugokencky, E. J., Masarie, K. A., Lang, P. M., & Tans, P. P. (1998). Continuing decline in the growth rate of the atmospheric methane burden. *Nature*, *393*(6684), 447–450. https://doi.org/10.1038/30934

Flannaghan, T. J., & Fueglistaler, S. (2013). The importance of the tropical tropopause layer for equatorial Kelvin wave propagation. *Journal of Geophysical Research: Atmospheres*, *118*, 5160–5175. https://doi.org/10.1002/jgrd.50418

Forster, P. M. F., & Shine, K. P. (1999). Stratospheric water vapour changes as a possible contributor to observed stratospheric cooling. *Geophysical Research Letters*, *26*(21), 3309–3312. https://doi.org/10.1029/1999GL010487

Forster, P. M. F., & Shine, K. P. (2002). Assessing the climate impact of trends in stratospheric water vapor. *Geophysical Research Letters*, *29*(6), 1086. https://doi.org/10.1029/2001GL013909

Fueglistaler, S., Bonazzola, M., Haynes, P. H., & Peter, T. (2005). Stratospheric water vapor predicted from the Lagrangian temperature history of air entering the stratosphere in the tropics. *Journal of Geophysical Research*, *110*, D08107. https://doi.org/10.1029/2004JD005516

Fueglistaler, S., Dessler, A. E., Dunkerton, T. J., Folkins, I., Fu, Q., & Mote, P. W. (2009). Tropical tropopause layer. *Reviews of Geophysics*, *47*, RG1004. https://doi.org/10.1029/2008RG000267

Fueglistaler, S., & Haynes, P. H. (2005). Control of interannual and longer-term variability of stratospheric water vapor. *Journal of Geophysical Research*, *110*, D24108. https://doi.org/10.1029/2005JD006019

Gettelman, A., Salby, M. L., & Sassi, F. (2002). Distribution and influence of convection in the tropical tropopause region. *Journal of Geophysical Research*, *107*(D10), 4080. https://doi.org/10.1029/2001JD001048

Gill, A. E. (1980). Some simple solutions for heat-induced tropical circulation. *Quarterly Journal of the Royal Meteorological Society*, *106*(449), 447–462. https://doi.org/10.1002/qj.49710644905

Hatsushika, H., & Yamazaki, K. (2003). Stratospheric drain over Indonesia and dehydration within the tropical tropopause layer diagnosed by air parcel trajectories. *Journal of Geophysical Research*, *108*(D19), 4610. https://doi.org/10.1029/2002JD002986

Hendon, H. H., & Salby, M. L. (1994). The life cycle of the Madden–Julian Oscillation. *Journal of the Atmospheric Sciences*, *51*(15), 2225–2237. https://doi.org/10.1175/1520-0469(1994)051%3C2225:TLCOTM%3E2.0.CO;2

Hendon, H. H., & Salby, M. L. (1996). Plandetary-scale circulations forced by intraseasonal variations of observed convection. *Journal of the Atmospheric Sciences*, *53*(12), 1751–1758. https://doi.org/10.1175/1520-0469(1996)053%3C1751:PSCFBI%3E2.0.CO;2

Highwood, E., & Hoskins, B. (1998). The tropical tropopause. *Quarterly Journal of the Royal Meteorological Society*, *124*(549), 1579–1604. https://doi.org/10.1002/qj.49712454911

Holloway, C. E., & Neelin, J. D. (2007). The convective cold top and quasi equilibrium. *Journal of the Atmospheric Sciences*, *64*(5), 1467–1487. https://doi.org/10.1175/JAS3907.1

Holton, J. R., & Gettelman, A. (2001). Horizontal transport and the dehydration of the stratosphere. *Geophysical Research Letters*, *28*(14), 2799–2802. https://doi.org/10.1029/2001GL013148

Holton, J. R., Haynes, P. H., McIntyre, M. E., Douglass, A. R., Rood, R. B., & Pfister, L. (1995). Stratosphere-troposphere exchange. *Reviews of Geophysics*, *33*(4), 403–439. https://doi.org/10.1029/95RG02097

Hoskins, B. J., McIntyre, M. E., & Robertson, A. W. (1985). On the use and significance of isentropic potential vorticity maps. *Quarterly Journal of the Royal Meteorological Society*, *111*(470), 877–946. https://doi.org/10.1002/qj.49711147002

Huffman, G. J., Bolvin, D. T., Nelkin, E. J., Wolff, D. B., Adler, R. F., Gu, G., … Stocker, E. F. (2007). The TRMM multisatellite precipitation analysis (TMPA): Quasi-global, multiyear, combined-sensor precipitation estimates at fine scales. *Journal of Hydrometeorology*, *8*(1), 38–55. https://doi.org/10.1175/JHM560.1

Jensen, E. J., Ackerman, A. S., & Smith, J. A. (2007). Can overshooting convection dehydrate the tropical tropopause layer? *Journal of Geophysical Research*, *112*, D11209. https://doi.org/10.1029/2006JD007943

Jensen, E., & Pfister, L. (2004). Transport and freeze-drying in the tropical tropopause layer. *Journal of Geophysical Research*, *109*, D02207. https://doi.org/10.1029/2003JD004022

Jensen, E. J., Ueyama, R., Pfister, L., Bui, T. V., Lawson, R. P., Woods, S., … Avery, M. A. (2016). On the susceptibility of cold tropical cirrus to ice nuclei abundance. *Journal of the Atmospheric Sciences*, *73*(6), 2445–2464. https://doi.org/10.1175/JAS-D-15-0274.1

Johnson, R. H., & Kriete, D. C. (1982). Thermodynamic and circulation characteristics of winter monsoon tropical mesoscale convection. *Monthly Weather Review*, *110*(12), 1898–1911. https://doi.org/10.1175/1520-0493(1982)110%3C1898:TACCOW%3E2.0.CO;2

Khaykin, S., Pommereau, J.-P., Korshunov, L., Yushkov, V., Nielsen, J., Larsen, N., … Williams, E. (2009). Hydration of the lower stratosphere by ice crystal geysers over land convective systems. *Atmospheric Chemistry and Physics*, *9*, 2275–2287. https://doi.org/10.5194/acp-9-2275-2009

Kiladis, G. N., Dias, J., Straub, K. H., Wheeler, M. C., Tulich, S. N., Kikuchi, K., … Ventrice, M. J. (2014). A comparison of OLR and circulation-based indices for tracking the MJO. *Monthly Weather Review*, *142*(5), 1697–1715. https://doi.org/10.1175/MWR-D-13-00301.1

Kiladis, G., Straub, K., Reid, G., & Gage, K. (2001). Aspects of interannual and intraseasonal variability of the tropopause and lower stratosphere. *Quarterly Journal of the Royal Meteorological Society*, *127*, 1961–1983.

Kim, J., & Son, S.-W. (2012). Tropical cold-point tropopause: Climatology, seasonal cycle, and intraseasonal variability derived from COSMIC GPS radio occultation measurements. *Journal of Climate*, *25*(15), 5343–5360. https://doi.org/10.1175/JCLI-D-11-00554.1

Kursinski, E. R., Hajj, G. A., Schofield, J. T., Linfield, R. P., & Hardy, K. R. (1997). Observing Earth's atmosphere with radio occultation measurements using the Global Positioning System. *Journal of Geophysical Research*, *102*(D19), 23,429–23,465. https://doi.org/10.1029/97JD01569

Lau, K.-H., & Lau, N.-C. (1990). Observed structure and propagation characteristics of tropical summertime synoptic scale disturbances. *Monthly Weather Review*, *118*(9), 1888–1913. https://doi.org/10.1175/1520-0493(1990)118%3C1888:OSAPCO%3E2.0.CO;2

Le Texier, H., Solomon, S., & Garcia, R. R. (1988). The role of molecular hydrogen and methane oxidation in the water vapour budget of the stratosphere. *Quarterly Journal of the Royal Meteorological Society*, *114*(480), 281–295. https://doi.org/10.1002/qj.49711448002

Liebmann, B., & Smith, C. A. (1996). Description of a complete (interpolated) outgoing longwave radiation dataset. *Bulletin of the American Meteorological Society*, *77*, 1275–1277.

Liu, C., & Zipser, E. J. (2008). Diurnal cycles of precipitation, clouds, and lightning in the tropics from 9 years of TRMM observations. *Geophysical Research Letters*, *35*, L04819. https://doi.org/10.1029/2007GL032437

Livesey, N., Read, W. G., Wagner, P. A., Froidevaux, L., Lambert, A., Manney, G. L., … Martinez, E. (2015). EOS MLS version 4.2x level 2 data quality and description document, Tech. Rep. Pasadena, CA: Jet Propulsion Laboratory, California Institute of Technology.

Mote, P. W., Rosenlof, K. H., McIntyre, M. E., Carr, E. S., Gille, J. C., Holton, J. R., … Waters, J. W. (1996). An atmospheric tape recorder: The imprint of tropical tropopause temperatures on stratospheric water vapor. *Journal of Geophysical Research*, *101*(D2), 3989–4006. https://doi.org/10.1029/95JD03422

Nishimoto, E., & Shiotani, M. (2012). Seasonal and interannual variability in the temperature structure around the tropical tropopause and its relationship with convective activities. *Journal of Geophysical Research*, *117*, D02104. https://doi.org/10.1029/2011JD016936

Paulik, L. C., & Birner, T. (2012). Quantifying the deep convective temperature signal within the tropical tropopause layer (TTL). *Atmospheric Chemistry and Physics*, *12*(24), 12,183–12,195. https://doi.org/10.5194/acp-12-12183-2012

Randel, W. J., & Jensen, E. J. (2013). Physical processes in the tropical tropopause layer and their roles in a changing climate. *Nature Geoscience*, *6*(3), 169–176. https://doi.org/10.1038/ngeo1733

Randel, W. J., & Wu, F. (2005). Kelvin wave variability near the equatorial tropopause observed in GPS radio occultation measurements. *Journal of Geophysical Research*, *110*, D03102. https://doi.org/10.1029/2004JD005006

Randel, W. J., Wu, F., Oltmans, S. J., Rosenlof, K., & Nedoluha, G. E. (2004). Interannual changes of stratospheric water vapor and correlations with tropical tropopause temperatures. *Journal of the Atmospheric Sciences*, *61*, 2133–2148. https://doi.org/10.1175/1520-0469(2004)061%3C2133:ICOSWV%3E2.0.CO;2

Randel, W. J., Wu, F., & Rios, W. R. (2003). Thermal variability of the tropical tropopause region derived from GPS/MET observations. *Journal of Geophysical Research*, *108*(D1), 4024. https://doi.org/10.1029/2002JD002595

Randel, W. J., Zhang, K., & Fu, R. (2015). What controls stratospheric water vapor in the NH summer monsoon regions? *Journal of Geophysical Research: Atmospheres*, *120*, 7988–8001. https://doi.org/10.1002/2015JD023622

Rossow, W. B., & Pearl, C. (2007). 22-Year survey of tropical convection penetrating into the lower stratosphere. *Geophysical Research Letters*, *34*, L04803. https://doi.org/10.1029/2006GL028635

Ryu, J.-H., Lee, S., & Son, S.-W. (2008). Vertically propagating Kelvin waves and tropical tropopause variability. *Journal of the Atmospheric Sciences*, *65*, 1817–1837. https://doi.org/10.1175/2007JAS2466.1

Sassen, K., & Wang, Z. (2008). Classifying clouds around the globe with the CloudSat radar: 1-year of results. *Geophysical Research Letters*, *35*, L04805. https://doi.org/10.1029/2007GL032591

Scherllin-Pirscher, B., Randel, W. J., & Kim, J. (2017). Tropical temperature variability and Kelvin wave activity in the UTLS from GPS RO measurements. *Atmospheric Chemistry and Physics*, *17*, 1–23. https://doi.org/10.5194/acp-2016-576

Schoeberl, M. R., & Dessler, A. E. (2011). Dehydration of the stratosphere. *Atmospheric Chemistry and Physics*, *11*(16), 8433–8446. https://doi.org/10.5194/acp-11-8433-2011

Schoeberl, M., Dessler, A., Ye, H., Wang, T., Avery, M., & Jensen, E. (2016). The impact of gravity waves and cloud nucleation threshold on stratospheric water and tropical tropospheric cloud fraction. *Earth and Space Science*, *3*(8), 295–305. https://doi.org/10.1002/2016EA000180

Schwartz, M. J., Read, W. G., Santee, M. L., Livesey, N. J., Froidevaux, L., Lambert, A., & Manney, G. L. (2013). Convectively injected water vapor in the North American summer lowermost stratosphere. *Geophysical Research Letters*, *40*, 2316–2321. https://doi.org/10.1002/grl.50421

Sherwood, S. C., & Dessler, A. E. (2000). On the control of stratospheric humidity. *Geophysical Research Letters*, *27*(16), 2513–2516. https://doi.org/10.1029/2000GL011438

Solomon, S., Rosenlof, K. H., Portmann, R. W., Daniel, J. S., Davis, S. M., Sanford, T. J., & Plattner, G.-K. (2010). Contributions of stratospheric water vapor to decadal changes in the rate of global warming. *Science*, *327*(5970), 1219–1223. https://doi.org/10.1126/science.1182488

Stephens, G. L., Vane, D. G., Boain, R. J., Mace, G. G., Sassen, K., Wang, Z., … CloudSat Science Team, T. (2002). The CloudSat mission and the a-train. *Bulletin of the American Meteorological Society*, *83*(12), 1771–1790. https://doi.org/10.1175/BAMS-83-12-1771

Stephens, G. L., Vane, D. G., Tanelli, S., Im, E., Durden, S., Rokey, M., … Marchand, R. (2008). CloudSat mission: Performance and early science after the first year of operation. *Journal of Geophysical Research*, *113*, D00A18. https://doi.org/10.1029/2008JD009982

Takashima, H., Eguchi, N., & Read, W. (2010). A short-duration cooling event around the tropical tropopause and its effect on water vapor. *Geophysical Research Letters*, *113*, D06107. https://doi.org/10.1029/2007JD009109

Virts, K. S., & Houze, R. A. (2015). Clouds and water vapor in the tropical tropopause transition layer over mesoscale convective systems. *Journal of the Atmospheric Sciences*, *72*(12), 4739–4753. https://doi.org/10.1175/JAS-D-15-0122.1

Virts, K. S., & Wallace, J. M. (2014). Observations of temperature, wind, cirrus, and trace gases in the tropical tropopause transition layer during the MJO*. *Journal of the Atmospheric Sciences*, *71*(3), 1143–1157. https://doi.org/10.1175/JAS-D-13-0178.1

Zhou, X., & Holton, J. R. (2002). Intraseasonal variations of tropical cold-point tropopause temperatures. *Journal of Climate*, *105*, 1460–1473.